FLUTTER OF RECTANGULAR SIMPLY SUPPORTED PANELS AT HIGH SUPERSONIC SPEEDS

by

John Mills Hedgepeth

Thesis submitted to the Graduate Faculty of the

Virginia Polytechnic Institute

in candidacy for the degree of

MASTER OF SCIENCE

in

Applied Mechanics

APPROVED:

Director of Graduate Studies

Dean of Engineering

APPROVED:

Head of Department

Major Professor

March 1957

Blacksburg, Virginia

TABLE OF CONTENTS

I. LIST OF FIGURES AND TABLES

II. INTRODUCTION

The aeroelastic instability of aircraft skin panels has been the subject of a number of theoretical investigations.[1-21] Most of these papers[1-16] have dealt in some detail with the problem of a one-dimensional panel in a two-dimensional flow and have been attempts either to establish approximate stability boundaries for use in the design of flat or slightly curved panels or to investigate some of the apparent peculiarities of the panel-flutter phenomenon. The aeroelastic behavior of thin cylinders has also been considered,[17,18] although in a somewhat preliminary fashion. In addition, the flutter of two-dimensional flat panels in a three-dimensional flow has been treated by Eisley[19] and Luke, St. John, and Gross[20,21]. It is to the latter subject that this thesis is directed.

The work both of Eisley and of Luke, St. John, and Gross concerns the flutter of rectangular simply supported plates subjected to supersonic flow over one side; both analyses employ modal solutions and present numerical results for a variety of panel aspect ratios for a limited range of supersonic Mach numbers. No attention is paid, however, either to the higher Mach numbers (greater than 2) or to the effects of midplane tension and compression stresses on flutter. In addition, neither analysis is completely satisfactory for an isolated panel; Eisley used linearized two-dimensional unsteady-flow theory and Luke, et al, while employing three-dimensional theory, actually solve the problem of an infinite-span panel separated into rectangular bays by equally spaced, rigid streamwise stiffeners.

In this thesis we consider again the flat rectangular simply supported plate. The important departure from the previous analyses is in the use of so-called "static" air forces,[2] for solving the flutter problem. Experience has shown that this static approximation yields flutter boundaries that exhibit excellent agreement with those yielded by more refined (with regard to unsteady effects) aerodynamic theories provided that the Mach number is sufficiently high.* The use of the static air forces has the obvious virtue of simplicity and allows the inclusion of three-dimensional aerodynamic forces in a relatively simple manner. In addition, large ranges of the pertinent parameters of the problem can be readily investigated. Also, studies of the effects on the flutter boundaries of the midplane stresses which might arise as a result of loading and aerodynamic heating are feasible.

Because of the paucity of experimental information pertaining to the flutter of flat, unbuckled panels, it is not possible to assess the overall accuracy of any panel flutter theory. Consequently, statements regarding the validity of the theory contained herein are based on comparisons with more refined (and, presumably, more accurate) theories.

The help of Prof. Daniel Frederick in preparing this thesis is hereby acknowledged. Appreciation is also due to Miss Lillie Belle Evans and Mr. Keith Redner of the staff of the National Advisory Committee for Aeronautics for their valuable aid in performing the numerical computations.

---

*Comparisons presented in a subsequent section show that the lower limit on Mach number is somewhere between $\sqrt{2}$ and 2.

III. SYMBOLS

A	$R_x - 2n^2\pi^2(a/b)^2$
$\bar{A}$	$\bar{R}_x - 2n^2(a/b)^2$ (Note that flutter is usually most critical for $n = 1$)
B	$k^2 + n^2\pi^2(a/b)^2R_y - n^4\pi^4(a/b)^4$
$\bar{B}$	$\bar{k}^2 + n^2(a/b)^2\bar{R}_y - n^4(a/b)^4$
$\bar{B}_o$	$(a/b)^2\bar{R}_y - (a/b)^4$
$C(m,\sigma)$	integral defined by equation (A14)
D	plate stiffness, $Eh^3/12(1 - \mu^2)$
E	Young's modulus of elasticity
$I_{mn}, J_{mn}, K_{mn}, L_{mn}$	functions used in evaluation of generalized force (see Appendix)
$\bar{L}_{mn,rs}$	generalized force of (rs) mode on (mn) mode
M	Mach number
N_x, N_y	midplane stresses (positive in compression)
R_x	N_xa^2/D
R_y	N_ya^2/D
$\bar{R}_x$	R_x/π^2
$\bar{R}_y$	R_y/π^2
$S(m,\sigma)$	integral defined by equation (A10)
U	velocity of air flow
W_n	complex amplitude of panel vibration (see eq. (4))
a,b	dimensions of panel (see fig. 1)

c_{mn}	amplitude of (mn) mode (see eq. (19))
h	panel thickness
k	frequency parameter, $\omega a^2 \sqrt{\gamma h/D}$
$\bar{k}$	k/π^2
l	lateral aerodynamic loading
l_{mn}	lateral aerodynamic loading due to (mn) mode
j,m,n,r,s	integers
q	dynamic pressure, $\rho U^2/2$
t	time
w	lateral deflection of panel
x,y,z	Cartesian coordinates (see fig. 1)
x_1	x/a
β	$\sqrt{M^2 - 1}$
γ	mass density of plate
ε	mass ratio, $\rho a/\gamma h$
φ	perturbation velocity potential
λ	dynamic pressure parameter, $2qa^3/\beta D$
λ_{cr}	critical value of λ
λ_T	transtability value of λ
μ	Poisson's ratio
ρ	mass density of air
σ	$\frac{m}{n}\frac{\beta b}{a}$
ω	circular frequency
$1(y)$	step function, equal to zero for $y < 0$ and equal to unity for $y > 0$

IV. STATEMENT OF PROBLEM

The configuration to be analyzed herein is shown in Figure 1. It consists of a simply supported flat plate of uniform thickness h mounted in a rigid wall with air flowing over the top at a Mach number M. The plate has a length a and a width b and is subjected to constant midplane force intensities N_x and N_y (positive in compression).

In the following analysis, small-deflection thin-plate theory is assumed to apply. The appropriate equilibrium equation and boundary conditions are:

$$D\nabla^4 w + N_x w_{xx} + N_y w_{yy} + \gamma h w_{tt} = l(x,y,t) \tag{1}$$

$$w(x,0,t) = w(x,b,t) = w(0,y,t) = w(a,y,t) = 0$$

$$w_{yy}(x,0,t) = w_{yy}(x,b,t) = w_{xx}(0,y,t) = w_{xx}(a,y,t) = 0$$

where $w(x,y,t)$ is the lateral deflection of the plate and $l(x,y,t)$ is the lateral load per unit area due to aerodynamic pressures; D is the plate stiffness $Eh^3/12(1-\mu^2)$ and γ is the density of the plate material.

As was mentioned in the Introduction we will assume that the air forces yielded by linearized static aerodynamic theory give an adequate approximation for this problem. In this theory, the loading at each instant is taken to be the loading which would result from flow over a stationary surface with a shape the same as the shape of

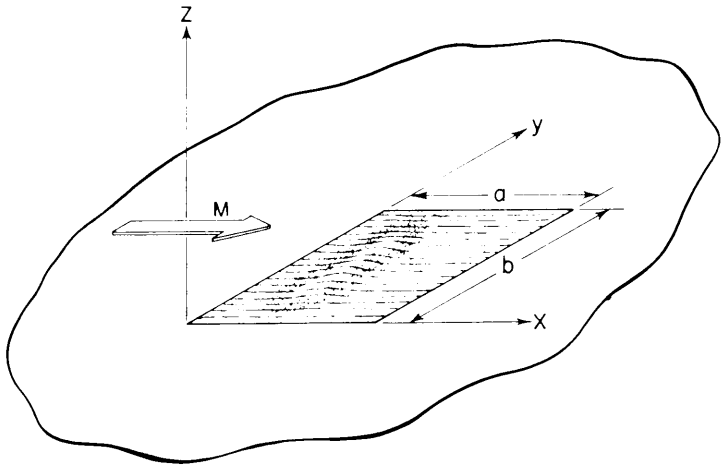

Fig. 1.- Rectangular panel and coordinate system.

the deflected plate at that instant. Thus no time-dependent effects are considered in either the potential equation, the boundary conditions, or the pressure-potential relations. Note that this differs (on the side of simplicity) from the so-called "quasi-steady" theory, in which time derivatives are included in the boundary conditions and pressure-potential relations and from the first-order theory[22] in which time-dependent effects are included approximately in all three governing relations.

As is usual in the treatment of flutter problems, the analysis contained herein is of the dynamic stability type. That is, conditions are sought for which an unstable (growing with time), self-excited motion is possible. The existence of such a possible motion would then imply instability of the panel since any small disturbance would "trigger" the motion.

In the following sections a closed-form solution of equation (1) is first carried out for two-dimensional aerodynamic theory (strip theory). The same problem is then solved by the Galerkin procedure in order to investigate the convergence of this modal approach. Finally, a modal solution of equation (1) for three-dimensional theory (surface theory) is presented.

V. ANALYSIS

Aerodynamic Strip Theory

For strip theory, the lateral loading is given by the simple Ackeret value

$$l(x,y,t) = -\frac{2q}{\beta} w_x(x,y,t) \tag{2}$$

where q is the dynamic pressure $\rho U^2/2$ and $\beta = \sqrt{M^2 - 1.}$ Equation (1) then becomes

$$D\nabla^4 w + N_x w_{xx} + N_y w_{yy} + \frac{2q}{\beta} w_x + \gamma h w_{tt} = 0 \tag{3}$$

For the simply supported plate a solution of equation (2) can be written in the form:

$$w = \mathrm{Re}\left[W_n(x) \sin \frac{n\pi y}{b} e^{i\omega t} \right] \tag{4}$$

The frequency ω is, in general, complex; however, we direct our attention primarily to real values of ω for which the motion is harmonic.

Substituting equation (4) into equation (3) and the associated boundary conditions and nondimensionalizing yields:

$$W_n^{IV} - 2n^2\pi^2\left(\frac{a}{b}\right)^2 W_n'' + n^4\pi^4\left(\frac{a}{b}\right)^4 W_n + R_x W_n'' - R_y n^2\pi^2\left(\frac{a}{b}\right)^2 W_n + \lambda W_n' - k^2 W_n = 0 \tag{5}$$

$$W_n(0) = W_n''(0) = W_n(1) = W_n''(1) = 0$$

where the primes denote differentiation with respect to $x_1 = x/a$ and

$$\left.\begin{aligned} R_x &= \frac{N_x a^2}{D} \\ R_y &= \frac{N_y a^2}{D} \\ \lambda &= \frac{2qa^3}{\beta D} \\ k^2 &= \frac{\gamma h a^4}{D}\omega^2 \end{aligned}\right\} \tag{6}$$

Equation (5) and the boundary conditions constitute an eigenvalue problem where k^2 can be considered to be the eigenvalue. We seek, in fact, the values of λ, R_x, and R_y for which one of the eigenvalues k^2 becomes complex and, hence, the panel becomes unstable. (See eq. (4).)

Equation (5) can be rewritten:

$$W_n^{IV} + AW_n'' + \lambda W_n' - BW_n = 0 \tag{7}$$

where

$$\left.\begin{aligned} A &= R_x - 2n^2\pi^2\left(\frac{a}{b}\right)^2 \\ B &= k^2 + n^2\pi^2\left(\frac{a}{b}\right)^2 R_y - n^4\pi^4\left(\frac{a}{b}\right)^4 \end{aligned}\right\} \tag{8}$$

Note that B now takes on the role of the eigenvalue.

Exact solution.- The characteristic equation for equation (7) is

$$p^4 + Ap^2 + \lambda p - B = 0$$

The roots of this equation can be written in the form[13]

$$p = -\alpha \pm \varepsilon, \quad \alpha \pm i\delta$$

where

$$\left.\begin{aligned} \delta &= \sqrt{\frac{\lambda}{4\alpha} + \alpha^2 + \frac{A}{2}} \\ \varepsilon &= \sqrt{\frac{\lambda}{4\alpha} - \alpha^2 - \frac{A}{2}} \\ B &= \frac{\lambda^2}{16\alpha^2} - 4\left(\alpha^2 + \frac{A}{4}\right)^2 \end{aligned}\right\} \tag{9}$$

Substituting the form

$$W_n = \sum_{i=1}^{4} D_i e^{p_i x_1}$$

in the boundary conditions yields the following condition for a nontrivial solution

$$\left[(\varepsilon^2 + \delta^2)^2 + 4\alpha^2(\delta^2 - \varepsilon^2)\right] \sin \delta \sinh \varepsilon = 8\alpha^2\varepsilon\delta(\cosh \varepsilon \cos \delta - \cosh 2\alpha) \tag{10}$$

The eigenvalue B can be computed for fixed values of λ and A by varying α until equation (10) is satisfied and then using the last

of equations (9) to determine B. The resulting solutions can be shown in the form of plots of λ versus B for various values of A. An example plot for A = 0 is indicated by the solid line in Figure 2. (The abscissa is $\sqrt[4]{B}/\pi$ instead of B in order to allow the inclusion of large ranges of B conveniently.)

It can be seen that for a fixed value of λ there exists an infinite discrete set of values of B. For $\lambda = 0$, the values of B can be shown to correspond to the natural frequencies of the plate in a vacuum. Increasing the dynamic-pressure parameter λ merely changes the values of B (and, hence, the natural frequencies) smoothly until a critical value (denoted λ_{cr} in Fig. 2) is reached. At this value, two of the roots for B become equal. For $\lambda < \lambda_{cr}$, the values of the frequencies remain real (provided the panel is unbuckled for $\lambda = 0$) and, thus, the panel is stable. For $\lambda > \lambda_{cr}$, two of the values of B become complex; hence, in view of equations (4), (6), and (8), the panel has at least one unstable mode of oscillation. Therefore, the value λ_{cr} defines the flutter boundary. (Note that other roots for B would coalesce and become complex if λ were increased further, thereby producing additional unstable modes. These secondary critical values are symbolized by the dotted lines in Fig. 2.)

The variation of λ_{cr} with A has been calculated and is shown by the solid line in Figure 3.* The abscissa here is

$$\bar{A} = \frac{A}{\pi^2} = \bar{R}_x - 2n^2\left(\frac{a}{b}\right)^2 \qquad (11)$$

*Some examples of the shape of the flutter mode are presented in the Appendix for interest.

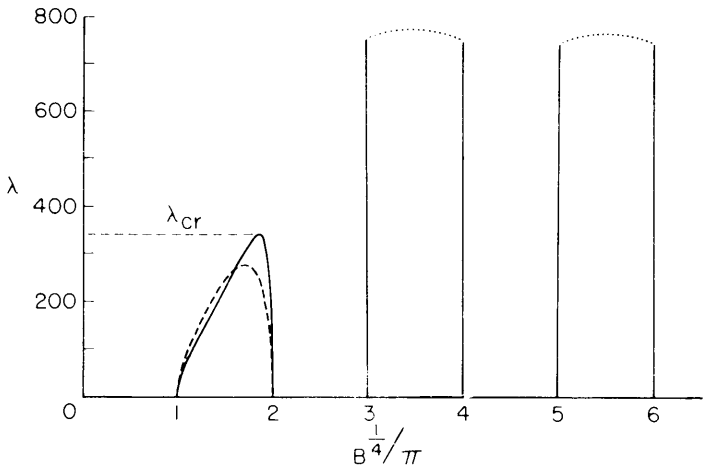

Fig. 2.- Influence of air flow on panel frequencies.

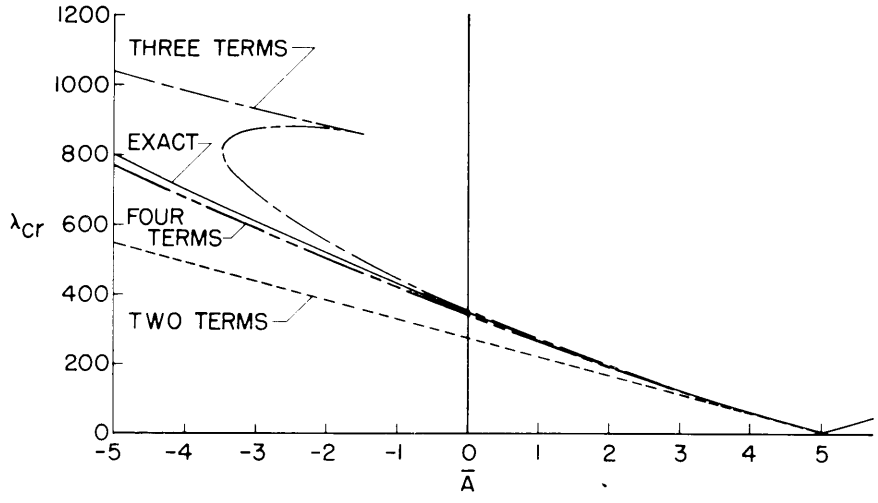

Fig. 3.- Variation of λ_{cr} with $\bar{A} = \bar{R}_x - 2n^2(a/b)^2$; strip-theory solution.

where

$$\bar{R}_x = \frac{R_x}{\pi^2} \tag{12}$$

Note that for $\bar{A} < 5$, λ_{cr} decreases monotonically with $\bar{A}$; thus, for fixed values of $\bar{R}_x$ and a/b, the lowest value of λ_{cr} would be achieved for $n = 1$. The resulting shape of the flutter mode in the y-direction would be a half sine wave.

Although a full discussion of the flutter boundary in Figure 3 is included in a later section of this thesis, a mention of several salient points is warranted here. The first is that the flutter speed is independent of R_y. This result, which comes about from the lack of coupling between the various modes in the y-direction, is of interest in connection with wing panels for which the greatest stress is usually in the spanwise (y) direction. Secondly, the range of validity of the results in Figure 3 is limited by the buckling characteristics of the plate. For instance, a square plate with no stress in the y-direction ($R_y = 0$) would buckle (for $\lambda = 0$) if $\bar{R}_x \geq 4$; for this reason, the curve in Figure 3 would be valid only for $\bar{A} < 2$.* Other values of a/b and R_y would yield other ranges of validity. Thirdly, the critical dynamic-pressure parameter is finite when the panel is on the verge of buckling even though the "effective stiffness" of the panel (as measured by the lowest in-vacuo natural frequency)

---

*Since the buckling load is affected by the air forces, this inequality is not strictly correct. This phenomenon is discussed in a later section.

approaches zero. Finally, the critical dynamic-pressure parameter goes to zero at $\bar{A}$ equal to 5. The need of large panel thicknesses if $\bar{A} \sim 5$ is obvious.

Galerkin solution.- In order to investigate the convergence of the modal procedure, a Galerkin solution of equation (7) will be performed.

Let

$$W_n = \sum_{m=1}^{j} c_{mn} \sin m\pi x_1$$

Substituting into equation (7), multiplying by $\sin r\pi x_1$, and integrating yields the following set of equations for the coefficients c_{mn}

$$\left(m^4 - m^2\bar{A} - \bar{B}\right)c_{mn} - \frac{\lambda}{\pi^3}\sum_{r=1}^{j} \bar{L}_{mn,rn}c_{rn} = 0 \qquad (m = 1,2,\ldots,j) \qquad (13)$$

where

$$\left.\begin{aligned} \bar{B} &= \frac{B}{\pi^4} = \frac{k^2}{\pi^4} + n^2\left(\frac{a}{b}\right)^2 R_y - n^4\left(\frac{a}{b}\right)^4 \\ \bar{L}_{mn,rs} &= \frac{4}{\pi}\frac{rm}{r^2 - m^2};\ n = s,\quad m + r \text{ odd} \\ \bar{L}_{mn,rs} &= 0;\ n = s,\quad m + r \text{ even} \\ \bar{L}_{mn,rs} &= 0;\ n \neq s \end{aligned}\right\} \qquad (14)$$

In the first of the latter expressions, $\bar{R}_y = R_y/\pi^2$. The seemingly overcomplicated form for the generalized aerodynamic-force coefficient $\bar{L}_{mn,rs}$ is introduced at this point to agree with the notation in the next section.

For a nontrivial solution, the determinant of the coefficients of c_{mn} must equal zero. If $j = 2$, for instance,

$$\begin{vmatrix} 1 - \bar{A} - \bar{B} & -\frac{8}{3\pi^4}\lambda \\ \frac{8}{3\pi^4}\lambda & 16 - 4\bar{A} - \bar{B} \end{vmatrix} = 0$$

Upon expanding and solving for λ we get

$$\lambda = \frac{3\pi^4}{8}\sqrt{(\bar{A} + \bar{B} - 1)(16 - 4\bar{A} - \bar{B})} \tag{15}$$

This relation is illustrated by the dashed line in Figure 2 for $\bar{A} = 0$. The two-term approximation to the critical value of λ can be obtained by finding the maximum; the result is

$$\lambda_{cr} = \frac{9\pi^4}{16}\left|5 - \bar{A}\right| \tag{16}$$

This approximation and the three-term and four-term approximations ($j = 3$ and 4) are compared in Figure 3 with the exact result. It can be seen that the two-term approximation consistently underestimates λ_{cr}, the error increasing as $\bar{A}$ becomes large negatively.

The three-term approximation is satisfactory for small values of $\bar{A}$ but is again unsatisfactory for the larger negative values of $\bar{A}$. On the other hand, the four-term solution yields good results over the entire range of $\bar{A}$ considered.*

Aerodynamic Surface Theory

The results in the preceding section were obtained on the basis of aerodynamic strip theory. The influence of three-dimensional aerodynamic effects on the flutter boundary is of interest. In this section, the flutter of the rectangular panel in a three-dimensional flow is analyzed by means of the Galerkin solution.

Air Forces.- The lateral loading due to the supersonic flow above the panel can be found in a straightforward manner by means of source-superposition techniques. Thus, if the deflection of the panel is $w(x,y,t)$, the lateral load $l(x,y,t)$ is[24]

$$l(x,y,t) = \rho U \frac{\partial \varphi}{\partial x}(x,y,t) \tag{17}$$

where

$$\varphi(x,y,t) = -\frac{U}{\pi} \iint \frac{\frac{\partial w}{\partial \xi}(\xi,\eta,t)\,d\xi\,d\eta}{\sqrt{(x-\xi)^2 - \beta^2(y-\eta)^2}} \tag{18}$$

The integration is carried out over the forward Mach cone from the point (x,y).

---

*It should be mentioned that the four-term solution would also be inaccurate for very large negative values of $\bar{A}$. In this case, the behavior of the plate approaches that of a membrane for which the Galerkin solution is known to be inapplicable.[23]

In the modal solution the deflection is expressed as the series

$$w = R_e \left[\sum_r \sum_s c_{rs} \sin \frac{r\pi x}{a} \sin \frac{s\pi y}{b} e^{i\omega t} \right] \tag{19}$$

in the region $0 \leq x \leq a$, $0 \leq y \leq b$. The corresponding loading is

$$l(x,y,t) = R_e \left[\sum_r \sum_s c_{rs} l_{rs}(x,y) e^{i\omega t} \right] \tag{20}$$

where

$$l_{rs}(x,y) = -2q \frac{r}{a} \frac{\partial}{\partial x} \int_0^x \int_{y-\frac{1}{\beta}(x-\xi)}^{y+\frac{1}{\beta}(x-\xi)} \frac{\cos \frac{r\pi\xi}{a} \sin \frac{s\pi\eta}{b}}{\sqrt{(x-\xi)^2 - \beta^2(y-\eta)^2}} \times$$

$$\left[1(\eta) - 1(\eta - b) \right] d\eta \, d\xi \tag{21}$$

Note that the step-function expression

$$1(\eta) - 1(\eta - b) = 0; \quad \eta < 0$$

$$= 1; \quad 0 < \eta < b$$

$$= 0; \quad \eta > b$$

excludes the regions outside of the plate from the integration.

Modal solution.- Substituting equations (19) and (20) into the equilibrium equation, equation (1), gives

$$\sum_r \sum_s \left\{ \left[D\left(\frac{r^2\pi^2}{a^2} + \frac{s^2\pi^2}{b^2}\right)^2 - N_x \frac{r^2\pi^2}{a^2} - N_y \frac{s^2\pi^2}{b^2} - \rho h\omega^2 \right] c_{rs} \sin\frac{r\pi x}{a} \sin\frac{s\pi y}{b} - c_{rs} l_{rs}(x,y) \right\} = 0$$

If this equation is multiplied by $\sin\frac{m\pi x}{a} \sin\frac{n\pi y}{b}$ and integrated, the result is

$$\left\{ \left[m^2 + n^2\left(\frac{a}{b}\right)^2 \right]^2 - m^2\bar{R}_x - n^2\left(\frac{a}{b}\right)^2\bar{R}_y - \bar{k}^2 \right\} c_{mn} = \frac{\lambda}{\pi^3} \sum_r \sum_s \bar{L}_{mn,rs} c_{rs} \tag{22}$$

where $\bar{k} = k/\pi^2$ and

$$\bar{L}_{mn,rs} = \frac{4\beta r}{\pi ab} \int_0^b \int_0^a \sin\frac{m\pi x}{a} \sin\frac{n\pi y}{b} \times \left\{ \frac{\partial}{\partial x} \int_0^x \int_{y-\frac{1}{\beta}(x-\xi)}^{y+\frac{1}{\beta}(x-\xi)} \frac{\cos\frac{r\pi\xi}{a} \sin\frac{s\pi\eta}{b}}{\sqrt{(x-\xi)^2 - \beta^2(y-\eta)^2}} \times \left[1(\eta) - 1(\eta - b) \right] d\eta\, d\xi \right\} dx\, dy$$

is the generalized force of the (rs) mode on the (mn) mode. Integration by parts yields

$$\bar{L}_{mn,rs} = \frac{4\beta mr}{a^2 b} \int_0^b \int_0^a \int_0^x \int_{y-\frac{1}{\beta}(x-\xi)}^{y+\frac{1}{\beta}(x-\xi)} \frac{\cos \frac{m\pi x}{a} \sin \frac{n\pi y}{b} \cos \frac{r\pi \xi}{a} \sin \frac{s\pi \eta}{b}}{\sqrt{(x-\xi)^2 - \beta^2 (y-\eta)^2}} \times$$

$$\left[1(\eta) - 1(\eta - b)\right] d\eta \, d\xi \, dx \, dy \qquad (23)$$

Before continuing, it is necessary to determine these generalized forces. As is usual for supersonic-aerodynamic problems, the generalized forces can be shown to be functions of the modified aspect ratio parameter $\beta b/a$. For $\beta b/a \geq 1$, the reduction of the expression for $\bar{L}_{mn,rs}$ in terms of Bessel and Struve functions and two readily evaluated single numerical integrations is possible; this reduction is carried out in the Appendix. Values of $\bar{L}_{mn,rs}$ for $\beta b/a = 1, 2, 4$ and $m, n, r, s = 1, 2, 3, 4$ are given in Table 1. Also given are the values for the two-dimensional case ($\beta b/a = \infty$) obtained from equation (15).

It should be noted that $\bar{L}_{mn,rs} = 0$ when $n + s$ is odd. Thus, flutter modes are either symmetric ($n = 1, 3, \ldots$) or antisymmetric ($n = 2, 4, \ldots$) about the midspan. Also, the generalized force possesses the following symmetry properties

$$\bar{L}_{mn,rs} = \bar{L}_{ms,rn}$$

$$\bar{L}_{mn,rs} = \bar{L}_{rn,ms}; \; m + r \text{ even}$$

$$\bar{L}_{mn,rs} = -\bar{L}_{rn,ms}; \; m + r \text{ odd}$$

TABLE 1.- VALUES OF GENERALIZED FORCE

$\bar{I}_{mn,rs}$

(a) $\frac{\beta b}{a} = 1$

mn \ rs	11	21	31	41	13	23	33	43
11	0.280799	0.918988	-0.016794	0.342534	-0.094024	0.027056	0.071348	0.031672
21	-.918988	[illegible]	1.707919	.062653	-.027056	-.225040	-.179612	-.052123
31	-.016794	-1.707919	.070016	2.278778	.071348	.179612	-.003225	-.122558
41	-.342534	.062653	-2.278778	.044784	-.031672	-.052123	.122558	.115964
13	-.094024	.027056	.071348	.031672	.394360	.179035	-.317892	.271309
23	-.027056	-.225040	-.179612	-.052123	-.179035	1.583401	1.559517	-.499237
33	.071348	.179612	-.003225	-.122558	-.317892	-1.559517	2.256613	3.197349
43	-.031672	-.052123	.122558	.115964	-.271309	-.499237	-3.197349	1.281462

mn \ rs	12	22	32	42	14	24	34	44
12	0.517757	0.645152	-0.252472	0.248644	0.009251	0.158695	0.078655	-0.008104
22	-.645152	1.117025	1.969184	.023543	-.158695	-.286360	.033953	.178954
32	-.252472	-1.969184	.704846	2.752580	.078655	-.033953	-.482967	-.411662
42	-.248644	.023543	-2.752580	.216547	.008104	.178954	.411662	.030538
14	.009251	.158695	.078655	-.008104	.282384	.056501	-.085948	.269460
24	-.158695	-.286360	.033953	.178954	-.056501	1.227685	.376736	-.617150
34	.078655	-.033953	-.482967	-.411662	-.085948	-.376736	2.984986	2.125151
44	.008104	.178954	.411662	.030538	-.269460	-.617150	-2.125151	3.633424

TABLE 1.- VALUES OF GENERALIZED FORCE - Continued

(b) $\frac{\beta b}{a} = 2$

mn \ rs	11	21	31	41	13	23	33	43
11	0.115737	0.910125	0.022377	0.359008	-0.056992	-0.043405	-0.018266	-0.012048
21	-.910125	.036088	1.566619	.012605	.043405	.005858	-.019678	-.013284
31	.022377	-1.566619	.011487	2.205615	-.018266	.019678	.023348	.006047
41	-.359008	.012605	-2.205615	.008108	.012048	-.013284	-.006047	.003112
13	-.056992	-.043405	-.018266	-.012048	.550382	.889221	-.127630	.287169
23	.043405	.005858	-.019678	-.013284	-.889221	.724612	2.009013	.171298
33	-.018266	.019678	.023348	.006047	-.127630	-2.009013	.168138	2.429539
43	.012048	-.013284	-.006047	.003112	-.287169	.171298	-2.429539	.087475

mn \ rs	12	22	32	42	14	24	34	44
12	0.364129	0.985523	0.013831	0.362869	-0.080855	-0.031587	0.012926	0.010780
22	-.985523	.241190	1.729682	.078351	.031587	-.069568	-.098219	-.058536
32	.013831	-1.729682	.039044	2.269501	.012926	.098219	.068260	.010209
42	-.362869	.078351	-2.269501	.042120	-.010780	-.058536	-.010209	.015761
14	-.080855	-.031587	.012926	.010780	.569556	.593959	-.343632	.191677
24	.031587	-.069568	-.098219	-.058536	-.593959	1.339618	2.168749	.114766
34	.012926	.098219	.068260	.010209	-.343632	-2.168749	.637950	2.803101
44	-.010780	-.058536	-.010209	.015761	-.191677	.114766	-2.803101	1.332676

TABLE 1.- VALUES OF GENERALIZED FORCE - Continued

(c) $\frac{\beta b}{a} = 4$

mn \ rs	11	21	31	41	13	23	33	43
11	0.034825	0.870251	0.009766	0.347509	-0.010958	-0.010364	-0.006399	-0.004678
21	-.870251	.004086	1.535199	.001478	.010364	.006573	.001822	.001331
31	.009766	-1.535199	.003639	2.189341	-.006399	-.001822	.000368	-.000820
41	-.347509	.001478	-2.189341	.000993	.004678	.001331	.000820	.001416
13	-.010958	-.010364	-.006399	-.004678	.264711	.985087	.045301	.379360
23	.010364	.006573	.001822	.001331	-.985087	.093516	1.628193	.036687
33	-.006399	-.001822	.000368	-.000820	.045301	-1.628193	.017556	2.231651
43	.004678	.001331	.000820	.001416	-.379360	.036687	-2.231651	.019055

mn \ rs	12	22	32	42	14	24	34	44
12	0.130759	0.924487	0.031581	0.365621	-0.025207	-0.022327	-0.012470	-0.008832
22	-.924487	.026649	1.563657	.010435	.022327	.010974	-.000285	-.000247
32	.031581	-1.563657	.011365	2.206962	-.012470	.000285	.004495	.000228
42	-.365621	.010435	-2.206962	.006039	.008832	-.000247	-.000228	.002066
14	-.025207	-.022327	-.012470	-.008832	.405794	1.018790	.029144	.373036
24	.022327	.010974	-.000285	-.000247	-1.018790	.232938	1.740563	.086199
34	-.012470	.000285	.004495	.000228	.029144	-1.740563	.280215	2.264862
44	.008832	-.000247	-.000228	.002066	-.373036	.086199	-2.264862	.090980

TABLE 1.- VALUES OF GENERALIZED FORCE - Concluded

(d) $\frac{\beta b}{a} = \infty$

rs / mn	11	21	31	41	13	23	33	43
11	0	0.848826	0	0.339531	0	0	0	0
21	-.848826	0	1.527887	0	0	0	0	0
31	0	-1.527887	0	2.182696	0	0	0	0
41	-.339531	0	-2.182696	0	0	0	0	0
13	0	0	0	0	0	.848826	0	.339531
23	0	0	0	0	-.848826	0	1.527887	0
33	0	0	0	0	0	-1.527887	0	2.182696
43	0	0	0	0	-.339531	0	-2.182696	0

rs / mn	12	22	32	42	14	24	34	44
12	0	0.848826	0	0.339531	0	0	0	0
22	-.848826	0	1.527887	0	0	0	0	0
32	0	-1.527887	0	2.182696	0	0	0	0
42	-.339531	0	-2.182696	0	0	0	0	0
14	0	0	0	0	0	.848826	0	.339531
24	0	0	0	0	-.848826	0	1.527887	0
34	0	0	0	0	0	-1.527887	0	2.182696
44	0	0	0	0	-.339531	0	-2.182696	0

For $\beta b/a < 1$, a similar, but more complicated, reduction can be made. No results have been obtained for this case, however, primarily because they would be useful only for very low-aspect-ratio panels. For example, values of $\beta b/a < 1$ would correspond to Mach numbers less than $\sqrt{2}$ for a panel of unit aspect ratio. But, as will be demonstrated, the static aerodynamic theory cannot be expected to yield good results for this region.

Calculations for an example panel.- In view of the results obtained for the modal solution for strip theory, it is evident that the use of four modes in the x-direction should give satisfactory accuracy. In the y-direction, it is convenient to include two modes: $n = 1$, since this constituted the most critical value for the strip-theory solution; and $n = 3$, in order to include effects of spanwise coupling.

Equation (22) then becomes

$$\left\{\left[m^2 + n^2\left(\frac{a}{b}\right)^2\right]^2 - m^2\bar{R}_x - n^2\left(\frac{a}{b}\right)^2\bar{R}_y - \bar{k}^2\right\} c_{mn} = \frac{\lambda}{\pi^3}\sum_{r=1,2,3,4}\sum_{s=1,3}\bar{L}_{mn,rs}c_{rs} = 0 \qquad \begin{pmatrix} m = 1, 2, 3, 4 \\ n = 1, 3 \end{pmatrix}$$

For a nontrivial solution, the determinant of the coefficients of c_{mn} must be zero. When expanded, this determinant yields an eighth-order equation in $\bar{k}^2$ in which the coefficients are dependent on λ, $\bar{R}_x$, $\bar{R}_y$, and a/b. As before we seek the lowest value of λ for fixed

$\bar{R}_x$, $\bar{R}_y$, and a/b for which two of the eight roots for $\bar{k}^2$ become complex. (For $\lambda = 0$, all roots are obviously real.) The calculations have been carried out for $a/b = 1$ and for a number of values of $\bar{R}_x$ and $\bar{R}_y$. The following values for λ_{cr} were obtained:

For $\beta b/a = 1$

$\bar{R}_y$ \ $\bar{R}_x$	-4	-2	0	2	4	6	8
-4	822.0	647.7	480.0	322.8	179.6	54.38	46.63
-2		647.7	480.0	322.8	179.6	54.38	
0		647.7	480.0	322.8	179.6		
2		647.8	480.1	322.9			
4		648.0	480.3				

For $\beta b/a = 2$

$\bar{R}_y$ \ $\bar{R}_x$	-4	-2	0	2	4	6	8
-4	847.7	668.2	495.8	333.9	186.3	56.56	46.35
-2		668.2	495.8	333.9	186.3	56.56	
0		668.2	495.8	333.9	186.3		
2		668.2	495.8	333.9			
4		668.2	495.8				

For $\beta b/a = 4$

$\bar{R}_y$ \ $\bar{R}_x$	-4	-2	0	2	4	6	8
-4	859.8	676.9	502.5	338.6	189.1	57.55	49.39
-2		676.9	502.5	338.6	189.1	57.55	
0		676.9	502.5	338.6	189.1		
2		676.9	502.5	338.6			
4		676.9	502.5				

In the calculations for $\beta b/a = 1$, 2, and 4, an automatic high-speed digital computer was used. For each set of values for $\bar{R}_x$ and $\bar{R}_y$ the determinant was expanded for various selected values of λ. The resulting eighth-order equation in $\bar{k}^2$ was then solved. The critical value of λ was found by an interpolation procedure.

A significant outcome of these calculations is the virtual independence of λ_{cr} on the value of $\bar{R}_y$. Evidently the coupling between the various modes in the y-direction is slight, even for $\beta b/a = 1$. Since the coupling is so slight, it is improbable that the addition of more modes in the y-direction would change the results appreciably. Thus the tabulated values can be considered to be essentially correct.

The lack of dependence on $\bar{R}_y$ also suggests the possibility that the value of λ_{cr} is dependent only on the parameter

$$\bar{A} = \bar{R}_x - 2\left(\frac{a}{b}\right)^2$$

as it was for the strip-theory solution. If this were the case, the results for $a/b = 1$ could be extended to apply to other aspect ratios through the use of this parameter. As a check, the values of λ_{cr} were calculated for $a/b = 2$, $\bar{R}_x = 4$, $\bar{R}_y = 0$ and $a/b = 1/2$, $\bar{R}_x = -3.5$, $\bar{R}_y = 0$. For $\beta b/a = 1$, the resulting values of λ_{cr} are 647.7 and 626.6, respectively, in reasonable agreement with the tabulated value for $a/b = 1$, $\bar{R}_x = -2$, $\bar{R}_y = 0$. Thus, the extension can apparently be made. The variation of λ_{cr} with $\bar{A}$ is shown in Figure 4 for $\beta b/a = 1$, 2, 4, and ∞ (strip theory); the values are also given in Table 2. Note that for $\bar{A} = 5$, the critical dynamic-pressure parameter is zero for all values of $\beta b/a$.

The significant results of this thesis are embodied in Table 2. From this table, the critical values of λ for isolated rectangular simply supported panels can be found in terms of $\bar{A}$ for a large range of panel aspect ratio, midplane stress, and Mach number. The necessary panel thickness to prevent panel flutter can then be calculated from the value of λ_{cr}. In this regard, it is interesting to note that the aerodynamic effect of finite aspect ratio on the panel thickness is very small. For the range considered the variation of λ_{cr} between $\beta b/a = \infty$ and $\beta b/a = 1$ is approximately 6 percent; the corresponding variation of thickness would be less than 2 percent.

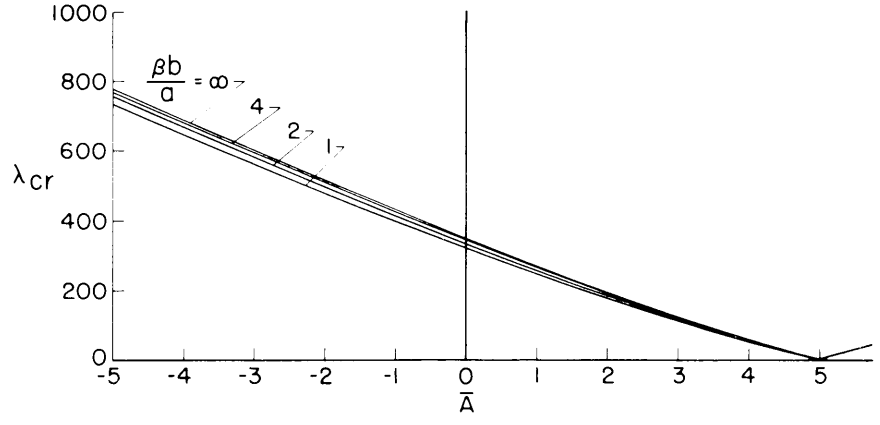

Fig. 4.- Variation of λ_{cr} with $\bar{A} = \bar{R}_x - 2(a/b)^2$; surface-theory solution.

TABLE 2.- CRITICAL VALUES OF DYNAMIC PRESSURE PARAMETER λ

$\bar{A}$ \ $\frac{\beta b}{a}$	1	2	4	∞
-6	822	848	860	863
-4	648	668	677	680
-2	480	496	502	505
0	323	334	339	341
2	179.6	186.3	189.1	190.3
4	54.4	56.6	57.6	58.0

VI. DISCUSSION

Accuracy of Static Aerodynamic Approximation

The results obtained by Eisley[19] by using linearized two-dimensional unsteady-flow theory provide an excellent basis for evaluating the accuracy of the static aerodynamic approximation employed in this thesis. The results calculated by a two-mode Galerkin solution for unstressed plates of aspect ratio 4, 2, 1, and 1/2 subjected to $M = 2$ flow are shown in Figure 5. The abscissa in this figure is the well-known mass ratio

$$\varepsilon = \frac{\rho a}{\gamma h}$$

which does not appear in the present analysis because of the simplicity of the aerodynamic theory. Indeed, the values of λ_{cr} obtained from the static approximation are the same as those in Figure 5 for $\varepsilon = 0$. It is therefore apparent that the static approximation is adequate if ε is small enough.

In order to define the practical range of ε, it is convenient to make use of the following combined parameter

$$\frac{\lambda}{\varepsilon^3} = 12(1 - \mu^2) \frac{\rho c^2}{E} \left(\frac{\gamma}{\rho}\right)^3 \frac{M^2}{\beta}$$

where c is the speed of sound in the air. Note that, for fixed Mach number, this parameter is dependent only on the properties of the air and the plate material. For a particular altitude-material combination,

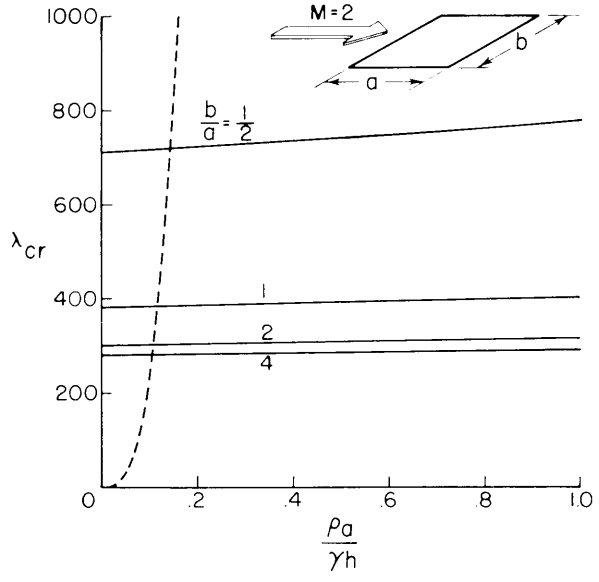

Fig. 5.- Results for M = 2 obtained from a two-mode strip-theory solution using unsteady air forces.

therefore, λ would vary as ϵ^3. The variation for magnesium at sea level is indicated by the dashed line in Figure 5. For this altitude-material combination the error of the static approximation can be seen to be negligible. For higher altitudes or denser materials the corresponding cubic line would lie above the one shown and the error would be less. It is reasonable to conclude, therefore, that the static approximation yields satisfactory accuracy for $M = 2$.

Investigations of the frequency expansions of the flutter forces (see ref. 6, for example) show that the accuracy of the static approximation would be even better for Mach numbers greater than 2. For $M < 2$, however, the accuracy decreases. At $\sqrt{M} = 2$, for instance, the unsteady flow theory yields two flutter boundaries[6,19] whereas the static theory predicts only one. It is probable, therefore, that a lower limit, somewhere between $\sqrt{2}$ and 2, exists on the Mach number range for which the results obtained in this thesis are applicable.

Buckling Behavior

It is generally agreed that buckling has an adverse effect on the flutter speed of panels. Past theoretical work on this subject, however, has dealt with only the two-dimensional panel-flutter problem. This work was pioneered by Isaacs[1], who introduced the concept of the "transtability" speed, a speed calculated from purely <u>static</u> considerations that constitutes an upper limit on the <u>flutter</u> speed of the buckled panel. Hayes[2] and Miles[3] then demonstrated that the transtability speed is indeed equal to the flutter speed for small perturbations about the static equilibrium position.

The similarity between the governing equations of two- and three-dimensional panel flutter for strip theory with static air forces (see eq. (7) and ref. 12) indicates that the flutter speed of a buckled finite-aspect-ratio panel might also be obtained through a transtability-type approach. A preliminary investigation, limited by the use of small-deflection plate theory to small buckle depths, of the static buckling behavior of panels is outlined here. Since some of the results obtained are of uncertain validity, being unsupported by a dynamic analysis, the investigation is limited to a two-mode solution for simplicity.

The effect of the air forces on the buckling load can be determined by setting $\bar{k}$ equal to zero in equation (15). Slightly rewritten, the equation becomes

$$\left(\frac{8\lambda}{3\pi^4}\right)^2 = \left(\bar{A} + \bar{B}_o - 1\right)\left(16 - 4\bar{A} - \bar{B}_o\right) \tag{24}$$

where, for $n = 1$

$$\bar{B}_o = \bar{R}_y\left(\frac{a}{b}\right)^2 - \left(\frac{a}{b}\right)^4$$

The buckling loads can be calculated from this equation. An example plot of the variation of $\bar{R}_x$ with λ for $a/b = 1$, $\bar{R}_y = 0$ is shown in Figure 6. Similar plots would result for other values of a/b and $\bar{R}_y$.

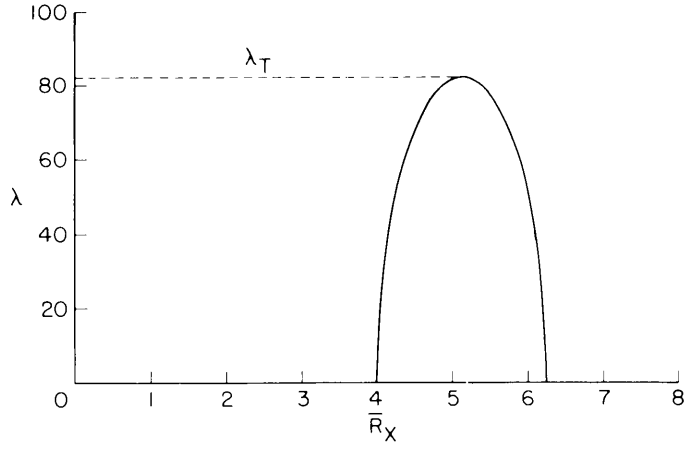

Fig. 6.- Influence of air flow on buckling loads for two-mode solution. $\bar{R}_y = 0$, $a/b = 1$.

The transtability analysis for the two-dimensional problem is based on a plot like that in Figure 6. It is argued that a buckled panel subjected to air flow would exhibit the midplane load given by the left-hand branch of the curve. If λ is increased, the load would increase until the maximum of the curve is reached. Further increase of λ would necessarily produce motion of the panel since there would be no stable static equilibrium position of the buckled panel. (Presumably, the panel would be unstable at the higher buckling loads not considered in the two-mode solution.) The maximum value of λ given by the curve is the transtability value.

The same line of reasoning can be used for the three-dimensional problem provided that the buckle depth is kept small. For this case, the results are dependent on the boundary conditions on in-plane deflections and stresses at the edges. Consider, for instance, a buckled panel with streamwise edges having a prescribed stress and spanwise edges having a prescribed displacement. For such boundary conditions the value of $\bar{B}_o$ would be fixed and the value of $\bar{A}$ would be that given by equation (24). The resulting transtability value of λ would be found from the condition

$$\frac{\partial \lambda}{\partial \bar{A}} = 0$$

which gives

$$\lambda_T = \frac{9\pi^4}{32}\left|4 + \bar{B}_o\right| \tag{25}$$

On the other hand, a panel with the edge boundary conditions reversed would have a fixed value of $\bar{A}$ and the appropriate transtability condition would be

$$\frac{\partial\lambda}{\partial\bar{B}_o} = 0$$

The resulting value of λ_T is

$$\lambda_T = \frac{9\pi^4}{16}\left|5 - \bar{A}\right| \tag{26}$$

which is the same as that obtained for the unbuckled panel (see eq. (16)); this result can, of course, be quite different from that given by equation (25).

In a practical situation, the edge boundary conditions would probably be different from either of the foregoing cases and different values of λ_T would result; each situation requires separate treatment.

A question might arise as to the usefulness of the small-deflection theory in obtaining results pertaining to finite-aspect-ratio buckled panels. It is felt, however, that such results represent correctly the limiting case of vanishingly small buckle depths and, furthermore, that this limiting case establishes a lower bound on the critical value of λ for buckled panels. The latter conjecture is based on the demonstrated independence of λ_{cr} on buckle depth for the two-dimensional problem[12,16] and the more rapid increase of stiffness with buckle depth for a finite-aspect-ratio plate than for an infinite-aspect-ratio plate (beam)[25]. A test of the validity of the conjecture,

and others implied in this section, must await a full-fledged dynamic analysis of the aeroelastic behavior of three-dimensional buckled panels including large-deflection structural effects.

Panel Thickness

Two examples of the variation of the critical thickness ratio with Mach number as obtained by the present theory are indicated by the solid lines in Figure 7. The results apply to unstressed aluminum panels at an altitude of 50,000 feet with aspect ratios of one and infinity. As could be expected, the effect of reducing the aspect ratio is to reduce the required h/a.

Also shown in Figure 7 are the results calculated from unsteady-flow theory for the lower supersonic Mach numbers by Luke and St. John[21]. These results, which are indicated by the dashed lines, merge well with the predictions of the present analysis. The meeting is nearly exact for the aspect ratio of infinity if account is taken of the fact that the dashed lines were obtained from a two-mode solution[21] whereas the solid lines were obtained from a four-mode solution; the effect of going from four to two modes is to increase the thickness by 7.5 percent. For the case of unit aspect ratio, the results are again not directly comparable; in addition to being based on fewer modes, the dashed line applies to a spanwise array of panels rather than to an isolated panel. The effect of this latter disparity is probably small for $M = 1.5$, however, since strip theory yields the same results for both configurations and the aerodynamic influence

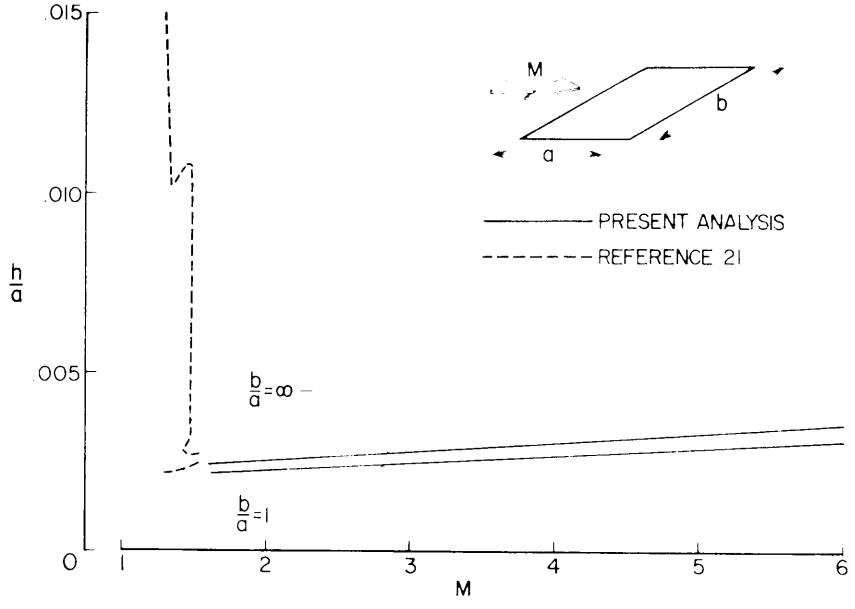

Fig. 7.- Variation of thickness ratio with Mach number for unstressed aluminum panels at 50,000 feet.

of finite aspect ratio is rather unimportant. The correction for number of modes mentioned above would again produce excellent agreement.

Past analyses of two-dimensional panel flutter have indicated that the most critical condition for design occurs at a value of Mach number of about 1.3. This is illustrated strikingly by the infinite-aspect-ratio curves in Figure 7. The required thickness decreases rapidly between $M = 1.3$ and 1.5 and then increases very slowly. Even at $M = 6$, the thickness ratio is only about one-fourth of that at $M = 1.3$. However, the situation is apparently different for finite aspect ratios; a virtually monotonic increase of required thickness with Mach number is experienced for an aspect ratio of one. Thus the high Mach number theory of this thesis should provide useful design information for panels of moderately low aspect ratio.

The numerical values of the critical thickness ratios in Figure 7 are fairly small and would be of consequence only for lightly loaded portions of the structure such as fairings and control surfaces. It should be emphasized, however, that large thickness ratios would be required if the parameter $\bar{A}$ were close to 5. This situation would not be difficult to attain. For instance, if a panel of aspect ratio equal to 1/2 were subjected to a compressive midplane stress in the chordwise direction only, $\bar{A} = 5$ could be achieved without buckling. Even for a panel of unit aspect ratio, $\bar{A} = 5$ could be obtained without buckling by compressing in the x-direction and pulling in the y-direction. It is obvious that such configurations should be assiduously avoided in design.

VII. CONCLUDING REMARKS

The panel flutter analysis presented herein has been restricted to the problem of an isolated simply supported plate of uniform thickness. The same type of analysis can be applied, however, to other panel configurations. Clamped panels, integrally stiffened panels, arrays of panels, and others should be amenable to treatment by the modal approach based on the static aerodynamic approximation.

It is generally agreed that flutter analyses should be supported by experiment. In this regard, the small amount of data[16,26] which is available indicates that theoretical panel-flutter calculations are somewhat conservative. Most of these data, however, relates either to buckled panels or to the lower supersonic Mach numbers. More experimental data, especially on unbuckled panels, are needed in order to assess the validity of panel-flutter analyses.

VIII. REFERENCES

[1]Isaacs, R. P., Transtability Flutter of Supersonic Aircraft Panels, U. S. Air Force Project RAND P-101, The Rand Corp., July 1, 1949.

[2]Hayes, W., A Buckled Plate in a Supersonic Stream, North American Aviation Report AL-1029, May 10, 1950.

[3]Miles, J. W., Dynamic Chordwise Stability at Supersonic Speeds, North American Aviation Report AL-1140, Oct. 18, 1950.

[4]Miles, J. W., On the Aerodynamic Instability of Thin Panels, Journal of The Aeronautical Sciences, Vol. 23, No. 8, pp. 771-780, August, 1956.

[5]Shen, S. F., Non-Stationary Aerodynamics of a Two-Dimensional Bump in a Uniform Stream and Its Effect on the Vibration Characteristics of an Elastic Panel, Massachusetts Institute of Technology, Contract No. N5ori-07833, Office Naval Res. (Project NR-064-259), May, 1952.

[6]Shen, S. F., Flutter of a Two-Dimensional Simply-Supported Uniform Panel in a Supersonic Stream, Massachusetts Institute of Technology, Contract No. N5ori-07833, Office Naval Res. (Project NR-064-259), August 6, 1952.

[7]Goland, M., and Luke, Y. L., An Exact Solution for Two-Dimensional Linear Panel Flutter at Supersonic Speeds, Readers Forum, Journal of the Aeronautical Sciences, Vol. 21, No. 4, pp. 275-276, April, 1954.

[8]Shen, S. F., Remarks on "An Exact Solution for Two-Dimensional Linear Panel Flutter at Supersonic Speeds", Readers Forum, Journal of The Aeronautical Sciences, Vol. 22, No. 9, pp. 656-657, September, 1955.

[9]Hedgepeth, J. M., Budiansky, B., and Leonard, R. W., Analysis of Flutter in Compressible Flow of a Panel on Many Supports, Journal of The Aeronautical Sciences, Vol. 21, No. 7, pp. 475-486, July, 1954.

[10]Nelson, H. C., and Cunningham, H. J., Theoretical Investigation of Flutter of Two-Dimensional Flat Panels with One Surface Exposed to Supersonic Potential Flow, NACA TN 3465, July, 1955.

[11]Fung, Y. C., The Static Stability of a Two-Dimensional Curved Panel in a Supersonic Flow, with an Application to Panel Flutter, Journal of The Aeronautical Sciences, Vol. 21, No. 8, pp. 556-565, August, 1954.

[12]Fung, Y. C., The Flutter of a Buckled Plate in Supersonic Flow, GALCIT Report No. OSR-TN-55-237, July, 1955.

[13]Hedgepeth, J. M., On the Flutter of Panels at High Mach Numbers, Readers Forum, Journal of the Aeronautical Sciences, Vol. 23, No. 6, pp. 609-610, June, 1956.

[14]Leonard, R. W., and Hedgepeth, J. M., On the Flutter of Infinitely Long Panels on Many Supports, To be published in the Readers Forum, Journal of The Aeronautical Sciences.

[15]Luke, Y. L., St. John, A. D., and Goland, M., An Exact Solution for Two-Dimensional Linear Panel Flutter at Supersonic Speeds, Midwest Research Institute, WADC TN 56-460, Contract No. AF 33(616)-2897, March 15, 1956,

[16]Eisley, J. G., The Flutter of a Two-Dimensional Buckled Plate with Clamped Edges in a Supersonic Flow, GALCIT Report No. OSR-TN-56-296, July, 1956.

[17]Miles, J. W., Supersonic Flutter of a Cylindrical Shell, Ramo-Wooldridge Corporation, Part I: General Theory, Report No. AM5-2, Aug. 19, 1955. Part II: Pressurization and Internal Fluid Effects, Report No. AM5-11, Nov. 14, 1955, Part III: Aeolotropic Shell, Report No. AM5-12, Dec. 2, 1955, Part IV: Effects of Non-Uniform Steady Flow, Report No. AM5-16, Dec. 7, 1955.

[18]Leonard, R. W., and Hedgepeth, J. M., On Panel Flutter and Divergence of Infinitely Long Unstiffened and Ring-Stiffened Thin-Walled Circular Cylinders, NACA TN 3638, April, 1956.

[19]Lisley, J. G., The Flutter of Simply Supported Rectangular Plates in a Supersonic Flow, GALCIT Report No. OSR-TN-55-236, July, 1955.

[20]Luke, Y. L., St. John, A. D., and Gross, B., Panel Flutter at Supersonic Speeds, Midwest Research Institute reports to WADC, Contract No. AF 33(616)-2897, Third Quarterly Progress Report, Mar. 29, 1956, Fourth Quarterly Progress Report, May 29, 1956.

[21]Luke, Y. L., and St. John, A. D., Panel Flutter at Supersonic Speeds, Midwest Research Institute, Fifth Quarterly Progress Report to WADC, Contract No. AF 33(616)-2897, Oct. 31, 1956.

[22]Miles, J. W., A First-Order Formulation of the Unsteady Supersonic Flow Problem for Finite Wings, Journal of the Aeronautical Sciences, Vol. 23, No. 6, pp. 578-582, June, 1956.

[23]Ashley, H., and Zartarian, G., Piston Theory - A New Tool for the Aeroelastician, Journal of The Aeronautical Sciences, Vol. 23, No. 12, pp. 1109-1118, Dec., 1956.

[24]Evvard, J. C., Use of Source Distributions for Evaluating Theoretical Aerodynamics of Thin Finite Wings at Supersonic Speeds, NACA Report 951, 1950.

[25]Bisplinghoff, R. L., and Pian, T. H. H., On the Vibrations of Thermally Buckled Bars and Plates, Massachusetts Institute of Technology, Contract No. N5ori-07833, Office Naval Research (Project NR-064-259), Sept., 1956.

[26]Sylvester, M. A., and Baker, J. E., Some Experimental Studies of Panel Flutter at Mach Number 1.3, NACA RM L52I16, Dec., 1952.

The vita has been removed from the scanned document

X. APPENDIX

EVALUATION OF $\bar{L}_{mn,rs}$

The generalized force $\bar{L}_{mn,rs}$ is given by equation (23)

$$\bar{L}_{mn,rs} = \frac{4\beta mr}{a^2 b} \int_0^b \int_0^a \int_0^x \int_{y-\frac{1}{\beta}(x-\xi)}^{y+\frac{1}{\beta}(x-\xi)} \times$$

$$\frac{\cos\frac{m\pi x}{a} \sin\frac{n\pi y}{b} \cos\frac{r\pi\xi}{a} \sin\frac{s\pi\eta}{b}}{\sqrt{(x-\xi)^2 - \beta^2(y-\eta)^2}} \times$$

$$\left[1(\eta) - (\eta - b)\right] d\eta\, d\xi\, dx\, dy \qquad \text{(A1)}$$

If ξ and η are replaced by

$$u = (x - \xi) - \beta(y - \eta)$$

$$v = (x - \xi) + \beta(y - \eta)$$

the result is

$$\bar{L}_{mn,rs} = \frac{2mr}{a^2 b} \int_0^{2a} \int_0^{2a-U} \frac{du\, dv}{uv} \int_0^b \sin\frac{n\pi y}{b} \sin\frac{s\pi}{b}\left(y - \frac{v-u}{2\beta}\right) \times$$

$$\left[1\left(y - \frac{v-u}{2\beta}\right) - 1\left(y - b - \frac{v-u}{2\beta}\right)\right] \times$$

$$dy \int_{\frac{u+v}{2}}^{a} \cos\frac{m\pi x}{a} \cos\frac{r\pi}{a}\left(x - \frac{u+v}{2}\right) dx \qquad \text{(A2)}$$

where the order of integration has been changed. Carrying out the x- and y-integrations yields the following result after some manipulation:

When $n + s$ is odd,

$$\bar{L}_{mn,rs} = 0 \tag{A3}$$

When $n + s$ is even,

$$\left.\begin{aligned}
\bar{L}_{mn,rs} &= \frac{4}{\pi^2} \frac{mnrs}{(r^2 - m^2)(s^2 - n^2)} (-1)^m (I_{rs} - I_{rn} - I_{ms} + I_{mn}) \qquad \begin{pmatrix} m \neq r \\ n \neq s \end{pmatrix} \\
&= \frac{2}{\pi^2} \frac{ns}{s^2 - n^2} (-1)^m (I_{ms} - I_{mn} - K_{ms} + K_{mn}) \qquad \begin{pmatrix} m = r \\ n \neq s \end{pmatrix} \\
&= \frac{2}{\pi^2} \frac{mr}{r^2 - m^2} (-1)^m (I_{mn} - I_{rn} - J_{rn} + J_{mn}) \qquad \begin{pmatrix} m \neq r \\ n = s \end{pmatrix} \\
&= \frac{1}{\pi^2} (-1)^m (-I_{mn} - J_{mn} + K_{mn} + L_{mn}) \qquad \begin{pmatrix} m = r \\ n = s \end{pmatrix}
\end{aligned}\right\} \tag{A4}$$

In these expressions

$$
\left.
\begin{aligned}
I_{mn} &= \frac{(-1)^m}{a}\,\frac{m}{n}\iint_R \frac{\sin m\pi\left(\frac{u+v}{2a}\right)\sin n\pi\left(\frac{v-u}{2\beta b}\right)}{\sqrt{uv}}\,du\,dv \\
J_{mn} &= \frac{(-1)^m}{a}\,m\pi\iint_R \frac{\left(1-\frac{v-u}{2\beta b}\right)\sin m\pi\left(\frac{u+v}{2a}\right)\cos n\pi\left(\frac{v-u}{2\beta b}\right)}{\sqrt{uv}}\,du\,dv \\
K_{mn} &= \frac{(-1)^m}{a}\,\frac{m^2\pi}{n}\iint_R \frac{\left(1-\frac{u+v}{2a}\right)\cos m\pi\left(\frac{u+v}{2a}\right)\sin n\pi\left(\frac{v-u}{2\beta b}\right)}{\sqrt{uv}}\,du\,dv \\
L_{mn} &= \frac{(-1)}{a}\,(m\pi)^2\iint_R \frac{\left(1-\frac{u+v}{2a}\right)\left(1-\frac{v-u}{2\beta b}\right)\cos m\pi\left(\frac{u+v}{2a}\right)\cos n\pi\left(\frac{v-u}{2\beta b}\right)}{\sqrt{uv}}\,du\,dv
\end{aligned}
\right\} \qquad (A5)
$$

The region of integration R is bounded by the lines $u = 0$, $u = v$, and $u + v = 2a$ for $\beta b/a \geq 1$ and by the additional line $v - u = 2\beta b$ for $\beta b/a < 1$.

Hereinafter we confine our attention to values of $\beta b/a$ greater than or equal to one. For this range the expressions for I_{mn}, J_{mn}, K_{mn}, and L_{mn} can be reduced to simpler forms as follows:

Let

$$
\left.
\begin{aligned}
u &= a\zeta(1 - \sin\theta) \\
v &= a\zeta(1 + \sin\theta)
\end{aligned}
\right\} \qquad (A6)
$$

Then I_{mn}, for example, becomes

$$I_{mn} = \frac{2m}{n}(-1)^m \int_0^{\frac{\pi}{2}} \int_0^1 \sin m\pi\zeta \, \sin\left(\frac{m\pi}{\sigma}\zeta \sin\theta\right) d\theta \, d\zeta \qquad (A7)$$

where

$$\sigma = \frac{m}{n}\frac{\beta b}{a} \qquad (A8)$$

Carrying out the ζ-integration yields

$$I_{mn} = -\frac{\sigma}{n\pi}\left[\int_0^{\frac{\pi}{2}} \frac{\sin\left(\frac{m\pi}{\sigma}\sin\theta\right)d\theta}{\sigma + \sin\theta} + \int_0^{\frac{\pi}{2}} \frac{\sin\left(\frac{m\pi}{\sigma}\sin\theta\right)d\theta}{\sigma - \sin\theta}\right]$$

or

$$I_{mn} = -\frac{\sigma}{n\pi}\left[S(m,\sigma) - S(m,-\sigma)\right] \qquad (A9)$$

where

$$S(m,\sigma) = \int_0^{\frac{\pi}{2}} \frac{\sin\left(\frac{m\pi}{|\sigma|}\sin\theta\right)d\theta}{\sin\theta + \sigma} \qquad (A10)$$

By a similar procedure we find

$$J_{mn} = \frac{\sigma}{\sigma^2 - 1}\frac{1}{n\pi}\left[S(m,\sigma) - S(m,-\sigma)\right] - \left[C(m,\sigma) - C(m,-\sigma)\right] +$$

$$\frac{\sigma}{\sigma^2 - 1}\frac{m}{n}\left[2 - \pi H_1\left(\frac{m\pi}{\sigma}\right)\right] \qquad (A11)$$

$$K_{mn} = -\frac{\sigma^3}{\sigma^2 - 1}\frac{1}{n\pi}\left[S(m,\sigma) - S(m,-\sigma)\right] - \frac{m}{n}\left[C(m,\sigma) + C(m,-\sigma)\right]$$

$$-\frac{\sigma}{\sigma^2 - 1}\frac{m}{n}\left[2 - \pi H_1\left(\frac{m\pi}{\sigma}\right)\right] \qquad (A12)$$

$$L_{mn} = \frac{3\sigma^3}{(\sigma^2 - 1)^2}\frac{1}{n\pi}\left[S(m,\sigma) - S(m,-\sigma)\right] + \sigma m\pi\left[S(m,\sigma) + S(m,-\sigma)\right]$$

$$-\frac{\sigma^3}{\sigma^2 - 1}\left[C(m,\sigma) - C(m,-\sigma)\right] + \frac{\sigma}{\sigma^2 - 1}\frac{m}{n}\left[C(m,\sigma) + C(m,-\sigma)\right]$$

$$+\frac{\sigma}{\sigma^2 - 1}m\pi^2 J_1\left(\frac{m\pi}{\sigma}\right) + \frac{\sigma(2 + \sigma)}{(\sigma^2 - 1)^2}\frac{m}{n}\left[2 - \pi H_1\left(\frac{m\pi}{\sigma}\right)\right] + \frac{2\sigma}{\sigma^2 - 1}\frac{m}{n}(-1)^m \qquad (A13)$$

where

$$C(m,\sigma) = \int_0^{\frac{\pi}{2}} \frac{\cos\left(\frac{m\pi}{\sigma}\sin\theta\right) - \cos m\pi}{\sin\theta + \sigma}\, d\theta \qquad (A14)$$

and J_1 and H_1 are Bessel and Struve functions.

The functions $S(m,\sigma)$ and $C(m,\sigma)$ can be evaluated accurately by means of numerical integration; the presence of the term $\cos m\pi$ in equation (A14) insures well-behaved integrands. For the calculations of the values of $L_{mn,rs}$ in Table 1, Gaussian integration with eight points on the interval $(0, \pi/2)$ was used; this procedure yields values of the integrals accurate to at least five significant figures.

Except in the special case $\beta = 1$, the values of $\bar{L}_{mn,rs}$ can be calculated from equations (A3), (A4), and (A9) through (A14). For $\beta = 1$, it is convenient to go back to equation (A5) and obtain expressions for I_{mn}, J_{mn}, K_{mn}, and L_{mn} directly. Thus, since $\frac{m\pi}{a} = \frac{n\pi}{\beta b}$ for this case, we can write, for example,

$$\sin m\pi\left(\frac{u+v}{2a}\right)\sin n\pi\left(\frac{v-u}{2\beta b}\right) = \frac{1}{2}\left(\cos\frac{m\pi u}{a} - \cos\frac{m\pi v}{a}\right)$$

and the necessary integrations can be performed without changing variables. The results for $\beta = 1$ are

$$\left.\begin{aligned}
I_{mn} &= \frac{m}{n}\left[2 - \pi H_1(m\pi)\right] \\
J_{mn} &= \frac{2}{3}\frac{m}{n} + \frac{1}{3}\frac{(m\pi)^2}{n}H_0(m\pi) - m\pi^2 J_1(m\pi) - \frac{2}{3}\frac{m\pi}{n}H_1(m\pi) \\
K_{mn} &= 2\frac{m}{n}(-1)^m - \frac{2}{3}\frac{m}{n} + \frac{2}{3}\frac{(m\pi)^2}{n}H_0(m\pi) - \frac{1}{3}\frac{m\pi}{n}H_1(m\pi) \\
L_{mn} &= \frac{2}{3}\frac{m}{n}(-1)^m + \frac{2}{15}\frac{m}{n} + \frac{2}{3}m^2\pi^3 J_0(m\pi) - \frac{1}{3}m\pi^2 J_1(m\pi) \\
&\quad - \frac{4}{15}\frac{m^3\pi^2}{n} + \frac{1}{5}\frac{(m\pi)^2}{n}H_0(m\pi) + \frac{m\pi}{n}\left(\frac{2}{15}m^2\pi^2 - \frac{2}{5}\right)H_1(m\pi)
\end{aligned}\right\} \quad (A15)$$

FLUTTER MODE SHAPES FOR AERODYNAMIC STRIP THEORY

The shape of the flutter mode as obtained from the exact solution of equation (7) is given by

$$W_n = \sum_{i=1}^{4} D_i \, e^{p_i x_1} \tag{A16}$$

where

$$p_{1,2,3,4} = -\alpha + \epsilon, -\alpha - \epsilon, \alpha + i\delta, \alpha - i\delta$$

The D_i must satisfy the matrix equation

$$\begin{bmatrix} 1 & 1 & 1 & 1 \\ e^{p_1} & e^{p_2} & e^{p_3} & e^{p_4} \\ p_1^2 & p_2^2 & p_3^2 & p_4^2 \\ p_1^2 e^{p_1} & p_2^2 e^{p_2} & p_3^2 e^{p_3} & p_4^2 e^{p_4} \end{bmatrix} \begin{vmatrix} D_1 \\ D_2 \\ D_3 \\ D_4 \end{vmatrix} = \begin{vmatrix} 0 \\ 0 \\ 0 \\ 0 \end{vmatrix} \tag{A17}$$

At flutter, of course, the determinant of the square matrix is zero and the D_i are determined except for a common multiplier. Thus, the set of D_i at flutter must be proportional to

$$D_1 = \begin{vmatrix} 1 & 1 & 1 \\ e^{p_2} & e^{p_3} & e^{p_4} \\ p_2^2 & p_3^2 & p_4^2 \end{vmatrix} i$$

$$D_2 = -\begin{vmatrix} 1 & 1 & 1 \\ e^{p_3} & e^{p_4} & e^{p_1} \\ p_3^2 & p_4^2 & p_1^2 \end{vmatrix} i$$

$$D_3 = \begin{vmatrix} 1 & 1 & 1 \\ e^{p_4} & e^{p_1} & e^{p_2} \\ p_4^2 & p_1^2 & p_2^2 \end{vmatrix} i$$

$$D_4 = -\begin{vmatrix} 1 & 1 & 1 \\ e^{p_1} & e^{p_2} & e^{p_3} \\ p_1^2 & p_2^2 & p_3^2 \end{vmatrix} i$$

where $i = \sqrt{-1}$ has been inserted as a multiplier in order to make the resulting W_n real.

The flutter mode shapes for $\bar{A} = -7, -3, 0, 3$ have been evaluated by using equation (A16) in conjunction with the appropriate values of λ and α. (See discussion following equation (10).) The results (normalized so that the maximum ordinates are unity) are shown in Figure 8. It can be seen that the amplitude of flutter is greatest in

the rear portion of the panel and that the peak amplitude moves rearward as $\bar{A}$ is decreased.

Also plotted in Figure 8 is the flutter mode shape as obtained by the two-term Galerkin solution. For this solution the shape is given by

$$W_n = \sin \pi x_1 - \sin 2\pi x_1 \qquad (A18)$$

for all values of $\bar{A}$. The degree of agreement with the exact shapes is similar to that shown in Figure 3 for λ_{cr}; that is, increasingly poor agreement with decreasing $\bar{A}$. The differences, however, are not as marked as those obtained for λ_{cr}.

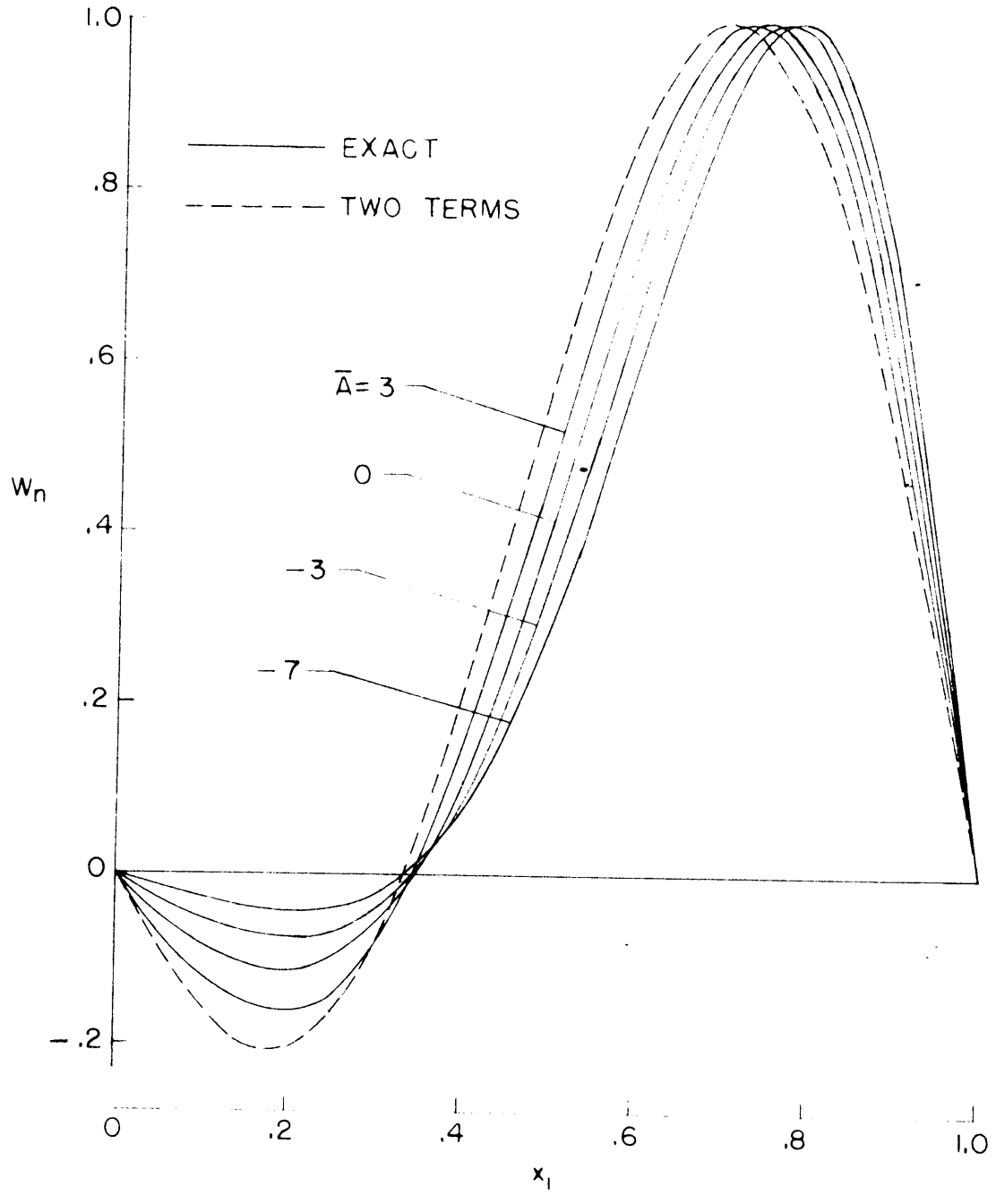

Figure 8. – Flutter Mode Shapes Obtained by Aerodynamic Strip Theory